Struct Multidisc Optim (2010) 41:189–203
DOI 10.1007/s00158-009-0418-9

RESEARCH PAPER

Improving the performance of simulated annealing in structural optimization

Oğuzhan Hasançebi · Serdar Çarbaş · Mehmet Polat Saka

Received: 12 November 2008 / Revised: 5 June 2009 / Accepted: 9 July 2009 / Published online: 7 August 2009

Abstract This study aims at improving the performance of simulated annealing (SA) search technique in real-size structural optimization applications with practical design considerations. It is noted that a standard SA algorithm usually fails to produce acceptable solutions to such problems associated with its poor convergence characteristics and incongruity with theoretical considerations. In the paper novel approaches are developed and incorporated into the standard SA algorithm to eliminate the observed drawbacks of the technique. The performance of the resulting (improved) algorithm is investigated in conjunction with two numerical examples (a 304-member braced planar steel frame, and 132-member unbraced space steel frame) designed according to provisions of the Allowable Stress Design (ASD) specification. In both examples, curves showing the variation of average acceptance probability parameter in standard and improved algorithms are plotted to verify usefulness and robustness of the integrated approaches.

Keywords Structural optimization · Discrete optimization · Metaheuristic search techniques · Simulated annealing · Steel frameworks

O. Hasançebi (✉)
Department of Civil Engineering,
Middle East Technical University,
06531 Ankara, Turkey
e-mail: oguzhan@metu.edu.tr

S. Çarbaş · M. P. Saka
Department of Engineering Sciences,
Middle East Technical University,
06531 Ankara, Turkey

1 Introduction

Kirkpatrick et al. (1983) used the so-called Metropolis algorithm to search for the best solution to an optimization problem amongst a set of feasible ones. In order to set forth the implicit connection between statistical mechanics and combinatorial optimization, they explained that in the annealing process minimization of the internal energy (heat) between many molecules was modeled using principles of statistical mechanics. Similarly, combinatorial optimization is the one such that it minimizes the value of an objective function between a number of design variables. They gave examples showing how statistical mechanics in annealing process was analogous to combinatorial optimization in designing computer chips as well as to the well-known traveling salesman problem. The technique, named simulated annealing (SA), soon gained a worldwide popularity as a metaheuristic search and optimization technique and found important applications in many disciplines of science and engineering.

Some relatively former applications of the technique in the realm of structural optimization and optimum control design have been reported in Balling (1991), Chen et al. (1991), Bennage and Dhingra (1995), Tzan and Pantelides (1996), and Shim and Manoochehri (1997). Amongst recent studies, Moh and Chiang (2000) developed an improved SA algorithm where design domain was successively reduced in the course of the search process. The minimum cost design of reinforced concrete retaining structures was studied in Ceramic et al. (2001) with SA. Hasançebi and Erbatur (2001) touched issues on efficient use of SA for complex structural optimization problems. Later in Hasançebi and Erbatur (2002), they developed a SA based solution algorithm for simultaneous optimum design of pin jointed structures, where the optimum size, shape and topology

of a structure was sought concurrently for minimizing its structural weight. Another efficiency improvement of the technique was attempted in Chen and Su (2002) based on two different strategies. In the first one a feasible region was estimated using linearized constraints and the algorithm was enforced to carry out a search in the estimated feasible region, whereas in the second one the search was initiated from a region of the design space having high values of design variables, and the search area was progressively moved towards the optimum in the subsequent iterations. In Erdal and Sönmez (2005), a set of current configurations was used rather than one trial point for maximizing bucking load capacity of composite laminates, and the approach was also found very effective for shape optimization of 2D structures in Sönmez (2007). Değertekin (2007) compared SA and genetic algorithm (GA) in optimum design of nonlinear space steel frames formulated according to AISC-LRFD (1986) specification. The study was concluded that SA outperformed GA for this class of problems. Finally, Lamberti (2008) implemented an advanced search mechanism with SA for optimizing trusses, where each candidate design was selected from a population of randomly generated trial points. It is clear from the above literature survey that ongoing research with SA is mostly concentrated on enhancing performance of the technique as well as on applying it to new problem areas.

This study is concerned with improvement of SA for structural optimization problems that consist of many design variables and constraints specified according to an actual design code. It is observed that a standard SA algorithm usually exhibits serious disadvantages when applied to such problems, resulting in poor convergence characteristics of the technique and inefficient search process. Two novel and generic approaches are introduced in the paper to eliminate the observed drawbacks of the standard algorithm. A reformulation of the acceptance probability parameter is proposed for non-improving solutions, plus degeneration of the search process by extremely poor solutions is avoided using a sigmoid function based update of the Boltzmann parameter. Two design examples are used mainly to test and compare numerical performances of the standard and improved SA algorithms. These examples are a 304-member braced planar steel frame and a 132-member unbraced space steel frame. In both examples the frames are sized for minimum weight considering stress, stability and displacement limitations according to the provisions of AISC-ASD (1989) specification. In addition, geometric constraints between beams and columns are considered for practicality of the solutions obtained. The curves representing the variation of average acceptance probability parameter in both standard and improved SA algorithms are plotted in each example to demonstrate the refinement of the search process with the proposed strategies.

2 Mathematical model of the optimization problem

For a steel structure consisting of N_m members that are collected in N_d design groups (variables), the optimum design problem according to AISC-ASD (1989) code yields the following discrete programming problem, if the design groups are selected from steel sections in a given profile list.

Find a vector of integer values $\mathbf{I}$ (1) representing the sequence numbers of steel sections assigned to N_d member groups

$$\mathbf{I}^T = \left[I_1, I_2, \ldots, I_{N_d}\right] \tag{1}$$

to minimize the weight (W) of the frame

$$W = \sum_{i=1}^{N_d} \rho_i A_i \sum_{j=1}^{N_t} L_j \tag{2}$$

where A_i and ρ_i are the area and unit weight of the steel section adopted for member group i, respectively, N_t is the total number of members in group i, and L_j is the length of the member j which belongs to group i.

The members subjected to a combination of axial compression and flexural stress must be sized to meet the following stress constraints:

$$if\ \frac{f_a}{F_a} > 0.15\ ;\ \left[\frac{f_a}{F_a} + \frac{C_{mx} f_{bx}}{\left(1 - \frac{f_a}{F'_{ex}}\right) F_{bx}} + \frac{C_{my} f_{by}}{\left(1 - \frac{f_a}{F'_{ey}}\right) F_{by}}\right] - 1.0 \le 0 \tag{3}$$

$$\left[\frac{f_a}{0.60 F_y} + \frac{f_{bx}}{F_{bx}} + \frac{f_{by}}{F_{by}}\right] - 1.0 \le 0 \tag{4}$$

$$if\ \frac{f_a}{F_a} \le 0.15\ ;\ \left[\frac{f_a}{F_a} + \frac{f_{bx}}{F_{bx}} + \frac{f_{by}}{F_{by}}\right] - 1.0 \le 0 \tag{5}$$

If the flexural member is under tension, then the following formula is used instead:

$$\left[\frac{f_a}{0.60 F_y} + \frac{f_{bx}}{F_{bx}} + \frac{f_{by}}{F_{by}}\right] - 1.0 \le 0 \tag{6}$$

In (3)–(6), F_y is the material yield stress, and $f_a = (P/A)$ represents the computed axial stress, where A is the cross-sectional area of the member. The computed flexural stresses due to bending of the member about its major (x) and minor (y) principal axes are denoted by f_{bx} and f_{by}, respectively. F'_{ex} and F'_{ey} denote the Euler stresses about principal axes of the member that are divided by a factory of safety of 23/12. F_a stands for the allowable axial

stress under axial compression force alone, and is calculated depending on elastic or inelastic bucking failure mode of the member using Formulas 1.5-1 and 1.5-2 given in AISC-ASD (1989). For an axially loaded bracing member whose slenderness ratio exceeds 120, F_a is increased by a factor of $(1.6 - L/200r)$ considering relative unimportance of the member, where L and r are the length and radii of gyration of the member, respectively. The allowable bending compressive stresses about major and minor axes are designated by F_{bx} and F_{by}, which are computed using the Formulas 1.5-6a or 1.5-6b and 1.5-7 given in AISC-ASD (1989). C_{mx} and C_{my} are the reduction factors, introduced to counterbalance overestimation of the effect of secondary moments by the amplification factors $\left(1 - f_a/F'_e\right)$. For unbraced frame members, they are taken as 0.85. For braced frame members without transverse loading between their ends, they are calculated from $C_m = 0.6 - 0.4\,(M_1/M_2)$, where M_1/M_2 is the ratio of smaller end moment to the larger end moment. Finally, for braced frame members having transverse loading between their ends, they are determined from the formula $C_m = 1 + \psi\left(f_a/F'_e\right)$ based on a rational approximate analysis outlined in AISC-ASD (1989) Commentary-H1, where ψ is a parameter that considers maximum deflection and maximum moment in the member.

For computation of allowable compression and Euler stresses, the effective length factors K are required. For beam and bracing members, K is taken equal to unity. For column members, alignment charts are furnished in AISC-ASD (1989) for calculation of K values for both braced and unbraced cases. In this study, however, the following approximate effective length formulas are used based on Dumonteil (1992), which are accurate to within about -1.0 and $+2.0\%$ of exact results (Hellesland 1994):

For unbraced members:

$$K = \sqrt{\frac{1.6G_AG_B + 4\,(G_A + G_B) + 7.5}{G_A + G_B + 7.5}} \tag{7}$$

For braced members:

$$K = \frac{3G_AG_B + 1.4\,(G_A + G_B) + 0.64}{3G_AG_B + 2.0\,(G_A + G_B) + 1.28} \tag{8}$$

where G_A and G_B refer to stiffness ratio or relative stiffness of a column at its two ends.

It is also required that computed shear stresses (f_v) in members are smaller than allowable shear stresses (F_v), as formulated in (9).

$$f_v \le F_v = 0.40C_vF_y \tag{9}$$

In (9), C_v is referred to as web shear coefficient. It is taken equal to $C_v = 1.0$ for rolled I-shaped members with $h/t_w \le 2.24E/F_y$, where h is the clear distance between flanges, E is the elasticity modulus and t_w is the thickness of web. For all other symmetric shapes, C_v is calculated from Formulas G2-3, G2-4 and G2-5 in ANSI/AISC 360-05 (2005).

Apart from stress constraints, slenderness limitations are also imposed on all members such that maximum slenderness ratio $(\lambda = KL/r)$ is limited to 300 for members under tension, and to 200 for members under compression loads. The displacement constraints are imposed such that the maximum lateral displacements are restricted to be less than $H/400$, and upper limit of story drift is set to be $h/400$, where H is the total height of the frame building and h is the height of a story.

Finally, we consider geometric constraints between beams and columns framing into each other at a common joint for practicality of an optimum solution generated. For the two beams B1 and B2 and the column shown in Fig. 1, one can write the following geometric constraints:

$$\frac{b_{fb}}{b_{fc}} - 1.0 \le 0 \tag{10}$$

$$\frac{b'_{fb}}{\left(d_c - 2t_f\right)} - 1.0 \le 0 \tag{11}$$

where b_{fb}, b'_{fb} and b_{fc} are the flange width of the beam B1, the beam B2 and the column, respectively, d_c is the depth of the column, and t_f is the flange thickness of the column. Equation (10) simply ensures that the flange width of the beam B1 remains smaller than that of the column. On the

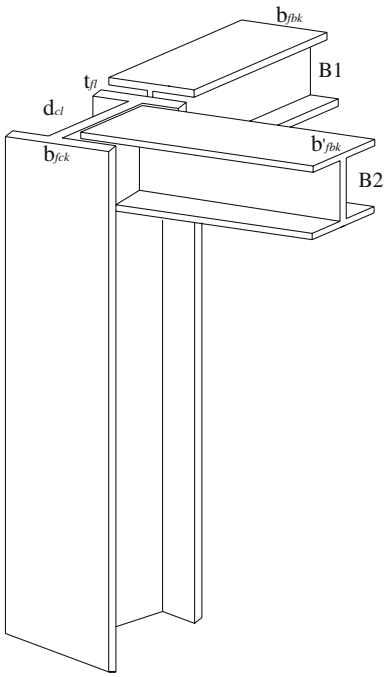

Fig. 1 Beam-column geometric constraints

other hand, (11) enables that flange width of the beam B2 remains smaller than clear distance between the flanges of the column ($d_c - 2t_f$).

3 Simulated annealing algorithm

The solution of the optimum design problem formulated in (1)–(11) necessitates the selection of appropriate steel sections for each member group (design variable) of the structure from the standard steel sections list. Hence, before initiating the design process, a set of steel sections selected from the available section list are collected in a design pool. Each steel section is then assigned a sequence number that varies between 1 to total number of sections in the list. During optimization process the selection of sections for member groups is carried out using these numbers. In the following, basic computational steps of a standard SA algorithm are outlined based on the enhancement of the technique for optimum structural design problems by Balling (1991). Various applications of this algorithm in structural optimization can be found in Balling (1991), Bennage and Dhingra (1995), Hasançebi and Erbatur (2001, 2002), Chen and Su (2002), Değertekin (2007), and Lamberti (2008).

Step 1. Cooling schedule The first step is the setting of an appropriate cooling schedule. After choosing suitable values for the starting acceptance probability (P_s), the final acceptance probability (P_f), and the number of cooling cycles (N_c), the cooling schedule parameters are calculated as follows:

$$T_s = -\frac{1}{\ln(P_s)}, \quad T_f = -\frac{1}{\ln(P_f)}, \quad \eta = \left[\frac{\ln(P_s)}{\ln(P_f)}\right]^{1/N_c - 1} \tag{12}$$

In (12), T_s, T_f and η are referred to as starting temperature, final temperature, and the cooling factor, respectively. The starting temperature is assigned as the current temperature of the process, i.e., $T = T_s$.

Step 2. Initial Design The next step is the generation of an initial design. The initial design is generated randomly such that each design variable represents the sequence number of the steel section selected from the profile list. This design is assigned as the current design of the optimization process. The analysis of the structure is performed with the standard steel sections selected in the current design and the force and deformation responses are obtained under the applied loads. If the design violates some of the problem constraints, it is penalized and its objective function value (ϕ_c) is calculated according to (13).

$$\phi = W\left[1 + \alpha\left(\sum_i g_i\right)\right] \tag{13}$$

In (13), ϕ is the constrained objective function value, g_i is the i-th problem constraint and α is the penalty coefficient used to tune the intensity of penalization as a whole. This parameter is set to an appropriate static value of $\alpha = 1$.

Step 3. Generating candidate designs A number of candidate designs are generated in the close vicinity of the current design. This is performed as follows: (a) a design variable (I_i) is selected, (b) the selected variable is given a small perturbation in a predefined neighborhood (14), and (c) finally, a candidate design is generated by assuming the perturbed value (I_i') of the variable, while keeping all others same as in the current design. It follows that a candidate design differs from the current one in terms of one design variable only. It is important to note that each design variable is selected only once in a random order to originate a candidate design. Hence, the total number of candidate designs generated in a single iteration of the cooling cycle is equal to the number of design variables.

$$I_i' = I_i \pm z_i \tag{14}$$

In (14), z_i refers to the amount of perturbation applied to the i-th design variable, and is sampled randomly within an integer neighborhood [1, n_w] specified, where n_w indicates the width of the neighborhood assigned to a constant value during optimization.

Step 4. Evaluating a candidate design and Metropolis test Each time when a candidate is generated, its objective function (ϕ_a) is computed according to (13) and is set to compete with the current design. If the candidate provides a better solution (i.e., $\Delta\phi = \phi_a - \phi_c \leq 0$), it is automatically accepted and replaces the current design. Otherwise, the so-called Metropolis test is resorted to determine the winner, in which the probability of acceptance of a poor candidate design (P) is assigned as follows:

$$P = \exp(-\Delta\phi / KT) \tag{15}$$

where K is referred to as Boltzmann parameter, and is manipulated as the working average of $\Delta\phi$ values during the search process. Hence, whenever a non-improving candidate is sampled, this parameter is updated as formulated as in (16), before its probability of acceptance is calculated in Metropolis test.

$$K^{(u)} = \frac{K^{(p)} N_a + \Delta\phi}{N_a + 1} \tag{16}$$

In (16), $K^{(p)}$is the Boltzmann parameter value before update; $K^{(u)}$ is the updated value of Boltzmann parameter, and N_a is the number of previous poor candidates. Metropolis test is finalized by generating a random number (r) between 0 and 1, such that if ($r \leq P$), the candidate is accepted and it replaces the current design. Otherwise ($r > P$), the candidate is rejected and the current design maintains itself.

Step 5. Iterations of a cooling cycle A single iteration of a cooling cycle is referred to the case where all design variables are selected once and perturbed to generate candidate designs. Generally, a cooling cycle is iterated a certain number of times in the same manner to ensure that objective function is reduced to a reasonably low value associated with the temperature of the cooling cycle. Having selected the iterations of the starting and final cooling cycles (i_s and i_f), the iteration of a cooling cycle (i_c) is determined by a linear interpolation between i_s and i_f, as follows:

$$i_c = i_f + (i_f - i_s)\left(\frac{T - T_f}{T_f - T_s}\right) \tag{17}$$

Step 6. Reducing temperature When the iterations of a cooling cycle are completed, the temperature is reduced by the ratio of the cooling factor η, and the temperature of the next cooling cycle is set.

$$T^{k+1} = T^k.\eta \tag{18}$$

In (18), T^k and T^{k+1} represent the temperatures at the k and $(k+1)$-th cooling cycles, respectively.

Step 7. Termination criterion The steps 3 through 6 are repeated until the whole cooling cycles are implemented.

4 Proposed strategies

In the following subsections the problems associated with the standard SA algorithm in optimum design of structural systems with many design variables and irregular design spaces are explained, and the strategies proposed to overcome these drawbacks are introduced.

4.1 Acceptance probability correction factor

The three main principles of the Metropolis test can be stated as follows: (a) due to elevated temperature in the beginning of the process, poor candidates are assigned high values of acceptance probability to facilitate design transitions for a thorough exploration of design space at early stages, (b) low values of $\Delta\phi$ (small uphill moves) are regarded more promising and thus higher acceptance probabilities are assigned to them in comparison to the large ones, and (c) when the temperature drops as the cooling proceeds, the probability of accepting uphill moves is reduced progressively towards zero so that toleration of the algorithm to transitions to infeasible or non-improving regions is aggravated in time to achieve a more exploitative search at later stages. These three principles of the Metropolist test play the major role in the success of the technique.

It is noted that Boltzmann parameter K is manipulated as the working average of $\Delta\phi$ values for non-improving candidates sampled in the optimization process, i.e., $K = \Delta\phi_{ave}$. Hence, it might be expected that if the acceptance probabilities of all candidates subjected to Metropolis test are averaged at each cooling cycle, the resulting values would follow the theoretical curve identified by the function $\exp(-1/T)$. As far as the optimum design of large structural systems is concerned, however, it is observed that such expectancy does not comply with the theoretical prospect at all. This situation is clearly illustrated in Fig. 2, which displays the variation of acceptance probability in a typical run with standard SA algorithm. It is seen from this figure that average acceptance probability in practice assumes much higher values than does the theory indicate when acceptance probabilities of poor candidates are calculated directly from (15). Since transitions to non-improving solutions are still tolerated to a large extent, convergence to a favourable design region cannot be achieved. To surmount this drawback of the standard algorithm, a reformulation of (15) has been considered in the present study, where a correction factor (ψ) is introduced as formulated in (19)–(20).

$$P = \psi.\exp(-\Delta\phi/KT) \tag{19}$$

$$\psi = \sqrt[3]{\frac{\overline{P}_t^{(k-1)}}{\overline{P}_p^{(k-1)}}}, \qquad 0.9 \leq \psi \leq 1.1 \tag{20}$$

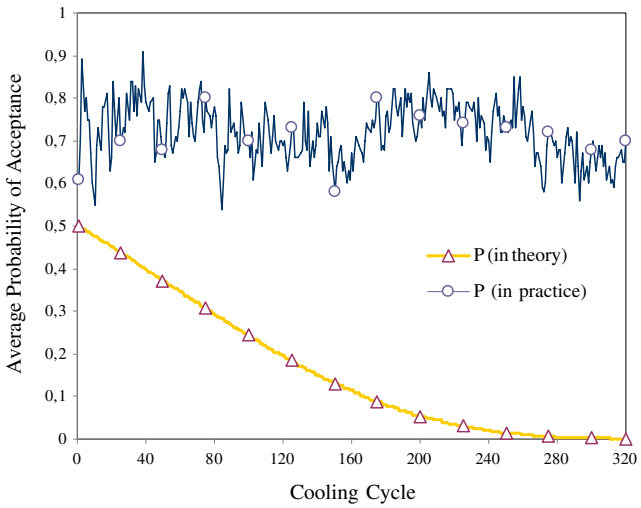

Fig. 2 Average acceptance probability (P) in practice and in theory

In (20), $\left(\overline{P}_t\right)^{(k-1)}$ and $\left(\overline{P}_p\right)^{(k-1)}$ represent the theoretical and practical (operational) average acceptance probabilities at the $(k-1)$-th cooling cycle, respectively. Accordingly, the acceptance probabilities of poor candidates at the k-th cooling cycle are modified based on the observed value of the ψ in the preceding cycle. By this way, it is ensured that acceptance probabilities assigned to poor candidates on average remain approximately in the same level with the theoretical idealization. The upper and lower bounds on the correction term ψ are imposed to facilitate a steady change in the value of this parameter in a controlled manner. Otherwise, immediate fluctuations would occur owing to rapid and highly irregular variation tendency of this parameter in successive cooling cycles.

4.2 Updating Boltzmann parameter using transformed $\Delta\phi$

Boltzmann parameter has the following functions that are of significance for a successful search process: (a) it serves to normalize $\Delta\phi$ values for the Metropolis test, which in turn enables a fruitful implementation of the algorithm irrespective of problem type; and (b) the search experience gained over the design space is stored in this parameter; and (c) this experience is then used to govern the acceptance criterion of the next candidates in connection with the formation of the previous ones. Note that while acceptance probability of an average poor candidate is $\exp(-1/T)$, this value decreases and increases for candidates with $\Delta\phi > K$ and $\Delta\phi < K$, respectively.

Occasionally, extremely poor candidate designs are generated and sampled in the natural course of the optimum design process. Such designs yield exceptionally high $\Delta\phi$ values that are far from reflecting general characteristics of the search space. A direct update of Boltzmann parameter as per such designs with (16) drives this parameter out of its usual range required for a successful process. Once this happens, the majority of subsequent candidates that are subjected to Metropolis test are accepted even if they produce substandard solutions, just because their $\Delta\phi$ values are lower than the operating value of Boltzmann parameter. The optimization turns into a random search process lacking necessary convergence characteristics. To this end, limiting the degree of infeasibility or inferiority (range of $\Delta\phi$) of poor candidates treated in Metropolis test is essential for an efficient implementation of Boltzmann parameter, although a direct interference to this parameter might be impractical or inefficient due to the lack of prior knowledge about the design space. To overcome this problem in a more efficient way, we consider transformation of $\Delta\phi$ values using the sigmoid function given in (21) and also shown graphically in Fig. 3, where $\Delta\phi_{tra}$ represents the transformed value of $\Delta\phi$.

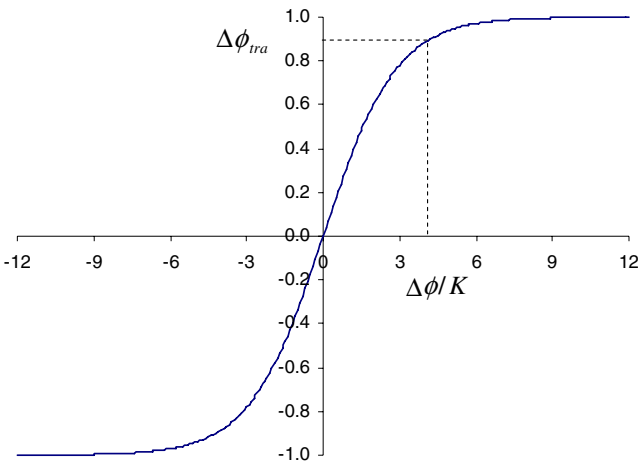

Fig. 3 Sigmoid transformation function

$$\Delta\phi_{tra} = \tanh\left(0.35 * \frac{\Delta\phi}{K}\right) \tag{21}$$

In this method, whenever a candidate design is generated, its $\Delta\phi$ value is first calculated in a usual manner and proportioned to the current value of Boltzmann parameter. Next, its transformed value $\Delta\phi_{tra}$ is calculated from (21). It can be observed from Fig. 3 that for all positive entries $(\Delta\phi/K)$ to the function, it returns a value between 0 and 1. It has a sensitive range for some values of $\Delta\phi/K$ (say between 0 and 6) over which the degree of weakness of a design is properly accounted for. Yet, as $\Delta\phi/K$ increases further, it becomes less and less sensitive to variations in $\Delta\phi/K$ and finally converges towards a value of 1.0 for the poorest candidates with $\Delta\phi >> K$. Hence, no matter how poor a candidate design is, the sigmoid function maps it to a limiting value of $\Delta\phi_{tra} = 1.0$ to make its degree of inferiority trivial after a point. Finally, acceptance probability of the candidate is computed from (22), where K_{tra} represents the working average of $\Delta\phi_{tra}$ values, i.e. $K = (\Delta\phi_{tra})_{ave}$.

$$P = \psi.\exp(-\Delta\phi_{tra}/K_{tra}T) \tag{22}$$

5 Numerical examples

Two numerical examples with practical design considerations are studied to test and compare performances of the standard and improved SA algorithms as well as to verify effectiveness of the proposed strategies. These examples are a 304-member braced planar steel frame and a 132-member unbraced space steel frame. They are designed for minimum weight considering cross-sectional areas of the members being the design variables. In both design examples, the following material properties of the steel are used: modulus of elasticity $(E) = 29{,}000$ ksi (203,893.6 MPa) and yield stress $(F_y) = 36$ ksi (253.1 MPa).

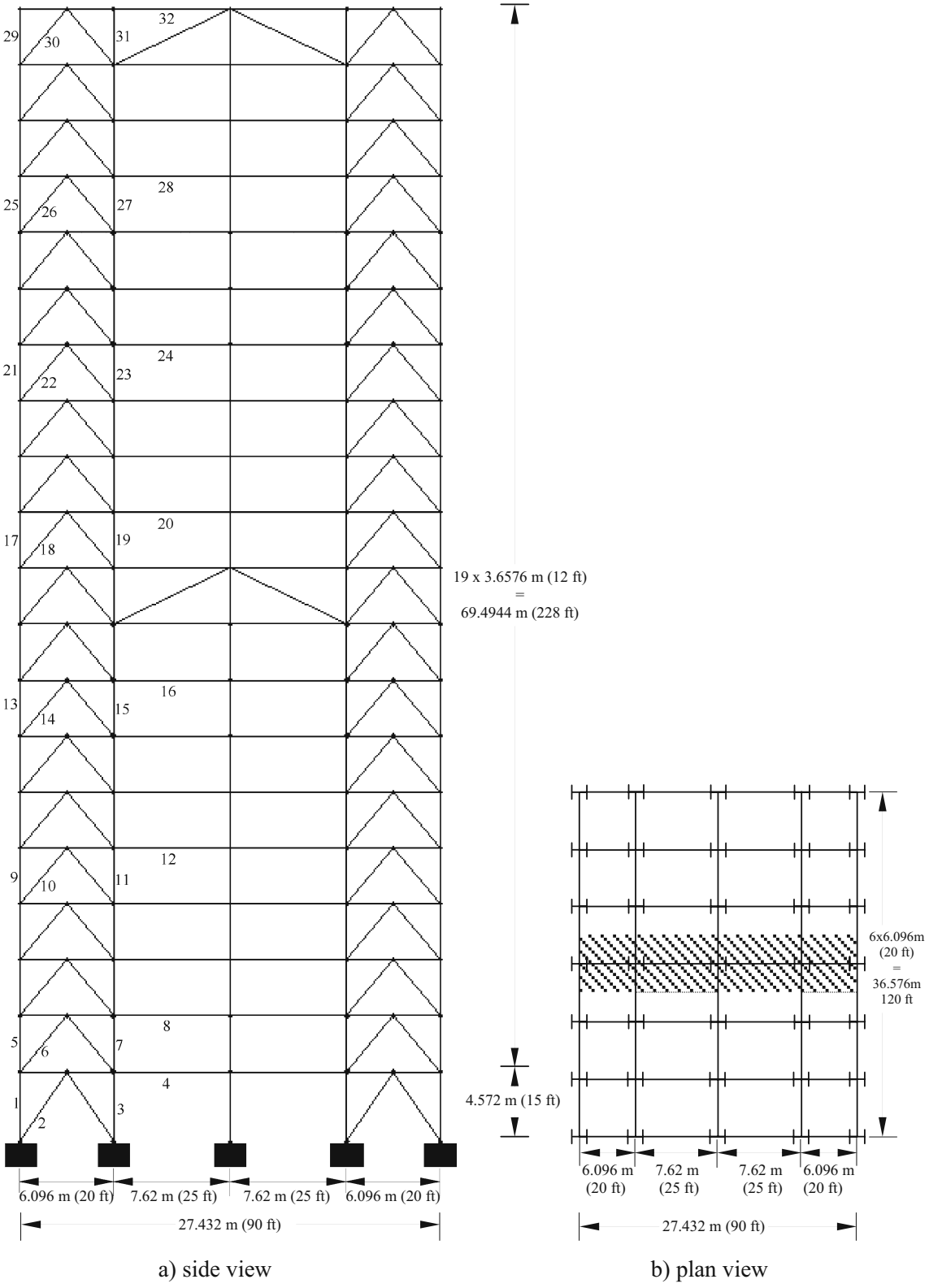

Fig. 4 304-member braced planar steel frame **a** side view, **b** plan view

Table 1 Gravity loading on the beams of 304-member braced planar steel frame

Beam type	Uniformly distributed load			
	Outer span beams		Inner span beams	
	(lb/ft)	(kN/m)	(lb/ft)	(kN/m)
Roof beams (dead + snow loads)	1,011.74	14.77	1,193.84	17.42
Floor beams (dead + live loads)	1,468.40	21.49	1,732.70	25.29

Solutions to these problems are also sought using two other metaheuristic search techniques, namely tabu search and harmony search methods in order to achieve comparability between the results of SA and other techniques. Tabu search (TS) is a metaheuristic search method originally developed by Glover (1989). The method implements a simple yet an efficient iterative based local search strategy for solving combinatorial optimization problems. At each step a number of candidate solutions are sampled in the close vicinity of the current design by perturbing a single design variable called a move. The best candidate is chosen and replaced with the current design even if it offers a non-improving solution, and the move leading to this candidate is recognized as a successful move. To protect the search against cycling within the same subset of solutions, information regarding most recently visited solutions is collected in a list referred to as tabu list. A candidate is allowed to replace the current design provided that its move is not in tabu list; otherwise the search is preceded with the current solution. Harmony search (HS) is another metaheuristic algorithm recently developed by Lee and Geem (2004). The method is based on natural musical performance processes that occur when a musician searches for a better state of harmony. The resemblance, for example between jazz improvisation that seeks to find musically pleasing harmony and the optimization is that the optimum design process seeks to find the optimum solution as determined by the objective function. The pitch of each musical instrument determines the aesthetic quality just as the objective function is determined by the set of values assigned to each design variable. The design algorithms developed for HS and TS methods are discussed in Hasançebi et al. (2009) with their complete computational steps.

5.1 Example 1: 304-member braced planar steel frame

Figure 4 shows plan and elevation views of a 20-story, 304-member braced (non-swaying) planar steel frame, which actually represents one of the interior frameworks of a steel building along the short side. It is assumed that all the beams and columns of the frame are rigidly connected, while the diagonals of K-braced truss are pin connected. The 304 members of the frame are grouped into 32 independent size variables to satisfy practical fabrication requirements. That is, except the first story exterior columns are grouped together as having the same section over three adjacent stories, as are interior columns, beams and diagonals, as indicated in Fig. 4. The complete wide-flange (W) profile list consisting of 297 ready sections is used to size column members, while beams and diagonals are selected from discrete sets of 171 and 147 economical sections selected from W-shape profile list based on area and inertia properties in the former, and on area and radii of gyration properties in the latter. The frame is subjected to a single loading

Table 2 Wind forces on 304-member braced planar steel frame

Floor no	Windward		Leeward	
	(lb)	(kN)	(lb)	(kN)
1	2,250.16	10.01	3,105.47	13.81
2	2,573.56	11.45	3,105.47	13.81
3	2,889.65	12.85	3,105.47	13.81
4	3,137.20	13.95	3,105.47	13.81
5	3,343.73	14.87	3,105.47	13.81
6	3,522.52	15.67	3,105.47	13.81
7	3,681.13	16.37	3,105.47	13.81
8	3,824.29	17.01	3,105.47	13.81
9	3,955.18	17.59	3,105.47	13.81
10	4,076.05	18.13	3,105.47	13.81
11	4,188.57	18.63	3,105.47	13.81
12	4,294.01	19.10	3,105.47	13.81
13	4,393.34	19.54	3,105.47	13.81
14	4,487.35	19.96	3,105.47	13.81
15	4,576.69	20.36	3,105.47	13.81
16	4,661.86	20.74	3,105.47	13.81
17	4,743.31	21.10	3,105.47	13.81
18	4,821.41	21.45	3,105.47	13.81
19	4,896.47	21.78	3,105.47	13.81
20	2,484.38	11.05	1,552.74	6.91

condition of combined gravity (dead, live and snow loads) and lateral (wind) loads that are computed as to ASCE 7-05 (2005) based on the following design values: a design dead load of 60.13 lb/ft^2 (2.88 kN/m^2), a design live load of 50 lb/ft^2 (2.39 kN/m^2), a ground snow load of 25 lb/ft^2 (1.20 kN/m^2) and a basic wind speed of 105 mph (65 m/s). The resulting gravity loads on the outer and inner beams of the roof and floors are listed in Table 1, and lateral (wind) loads acting at each floor level on windward and leeward faces of the frame are tabulated in Table 2. The combined stress and stability limitations of the members are calculated according to the provisions of AISC-ASD (1989), as explained in Section 2. In addition, the displacements of all nodes in any direction are restricted to a maximum value of 7.29 in (18.52 cm), which is equal to height of frame/400. Furthermore, story drift constraints are applied to each storey of the frame which is equal to height of each story/400.

The frame is optimized for minimum weight using three variants of the SA algorithm. In the first one the standard SA algorithm (sSA) is implemented as outlined in Section 3 using the following values of control parameters in line with the recommendations of the former studies (Balling 1991; Bennage and Dhingra 1995; Hasançebi and Erbatur 2001,

Table 3 Final best designs of 304-member braced planar steel frame obtained with iSA, TSO and HS methods

Size variables	iSA		TS		HS	
	Ready section	Area, cm^2(in^2)	Ready section	Area, cm^2(in^2)	Ready section	Area, cm^2(in^2)
1	W14X20	227.74 (35.3)	W14X132	250.32 (38.8)	W36X160	303.23 (47)
2	W30X191	361.94 (56.1)	W21X182	345.81 (53.6)	W18X192	363.87 (56.4)
3	W16X40	76.13 (11.8)	W18X40	76.13 (11.8)	W18X60	113.55 (17.6)
4	W8X24	45.68 (7.08)	W8X28	53.22 (8.25)	W12X58	109.68 (17)
5	W14X99	187.74 (29.1)	W21X111	210.97 (32.7)	W24X131	248.39 (38.5)
6	W18X175	330.97 (51.3)	W21X166	314.84 (48.8)	W27X194	367.74 (57)
7	W18X40	76.13 (11.8)	W16X45	85.81 (13.3)	W16X45	85.81 (13.3)
8	W8X24	45.68 (7.08)	W6X25	47.37 (7.34)	W8X28	53.23 (8.25)
9	W10X77	145.81 (22.6)	W12X79	149.68 (23.2)	W24X104	195.48 (30.6)
10	W21X147	278.71 (43.2)	W36X135	256.13 (39.7)	W21X132	250.32 (38.8)
11	W21X44	83.87 (13)	W18X46	87.10 (13.5)	W18X46	87.10 (13.5)
12	W6X25	47.35 (7.34)	W8X24	45.68 (7.08)	W12X30	56.71 (8.79)
13	W10X49	92.90 (14.4)	W10X54	101.94 (15.8)	W12X79	149.68 (23.2)
14	W33X118	223.87 (34.7)	W30X124	235.48 (36.5)	W18X119	226.45 (35.1)
15	W27X84	159.99 (24.8)	W27X84	159.99 (24.8)	W24X76	144.52 (22.4)
16	W10X60	113.55 (17.6)	W10X60	113.55 (17.6)	W10X60	113.55 (17.6)
17	W12X45	85.16 (13.2)	W10X45	85.81 (13.3)	W12X50	94.84 (14.7)
18	W21X101	192.26 (29.8)	W16X100	189.68 (29.4)	W24X104	195.48 (30.6)
19	W18X50	94.84 (14.7)	W18X55	104.51 (16.2)	W18X65	123.22 (19.1)
20	W6X15	28.58 (4.43)	W5X16	30.19 (4.68)	W8X21	39.74 (6.16)
21	W10X33	62.65 (9.71)	W8X31	58.90 (9.13)	W18X65	123.22 (19.1)
22	W12X58	109.68 (17)	W10X60	113.55 (17.6)	W18X71	134.18 (20.8)
23	W16X40	76.13 (11.8)	W18X40	76.13 (11.8)	W18X50	94.84 (14.7)
24	W6X15	28.58 (4.43)	W5X16	30.19 (4.68)	W8X18	33.94 (5.26)
25	W6X20	37.87 (5.87)	W6X20	37.87 (5.87)	W8X40	75.48 (11.7)
26	W12X40	76.13 (11.8)	W14X43	81.29 (12.6)	W21X62	118.06 (18.3)
27	W18X40	76.13 (11.8)	W18X40	76.13 (11.8)	W18X40	76.13 (11.8)
28	W6X15	28.58 (4.43)	W4X13	24.71 (3.83)	W6X25	47.35 (7.34)
29	W8X31	58.9 (9.13)	W8X31	58.90 (9.13)	W24X94	178.71 (27.7)
30	W8X31	58.9 (9.13)	W10X39	74.19 (11.5)	W10X60	113.55 (17.6)
31	W18X55	104.52 (16.2)	W18X55	104.51 (16.2)	W24X76	154.52 (22.4)
32	W8X31	58.9 (9.13)	W8X31	58.90 (9.13)	W12X40	76.13 (11.8)
Weight	232,811.88 lb	(105,603.47 kg)	236,586.49 lb	(107,315.63 kg)	269,055.45 lb	(122,043.55 kg)

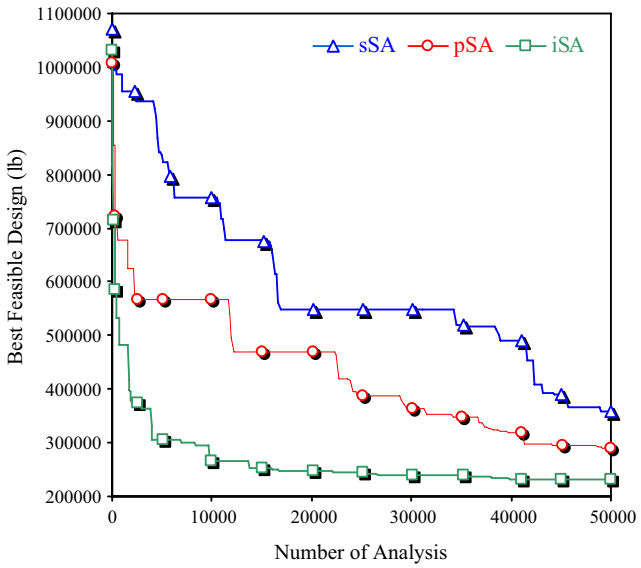

Fig. 5 The variation of feasible best design in sSA, pSA and iSA algorithms for 304-member braced planar steel frame

2002): $P_s = 0.50$, $P_f = 10^{-7}$, $i_s = 1$, $i_f = 7$, $n_w = 10$, $N_c = 320$. This led to the following cooling schedule parameters from (12): $T_s = 1.4427$, $T_f = 0.1448$ and $\eta = 0.9902$. In the second algorithm, to see the effect of sigmoid function transformation based update of Boltzmann parameter on the optimization process alone, this strategy is solely integrated into solution procedure. The resulting algorithm is referred to as partially improved SA (pSA) and is executed under the same values of parameter set with the former. Finally, both of the strategies developed in Section 4 are incorporated to yield the improved SA algorithm (iSA) proposed in the study. The improved SA is employed with the same values of the parameter set, except that final acceptance probability is set to $P_f = 10^{-3}$, which results in the following cooling schedule parameters: $T_s = 1.4427$, $T_f = 0.0620$ and $\eta = 0.9928$.

Considering stochastic nature of the technique, the frame is separately designed a number of times with each SA algorithm, and the best performance is considered. The sSA algorithm performed very poorly and located a final design weight of 357,358.91 lb (162,098.00 kg) that is very far from the optimum solution of the problem. This design has been improved to a certain extent with pSA, which obtained a final design weight of 289,914.76 lb (131,505.34 kg) that could still be treated as poor. Compared to these two solutions, the iSA algorithm yielded a much better design that weighs 232,811.88 lb (105,603.47) only. This design is tabulated in Table 3 with section designations attained for each member group. In all the cases a total of approximately 50,000 function evaluations (structural analyses) were performed to reach the final designs reported above. In an effort to compare the solution of iSA with those of other metaheuristic technqiues, the same example has been studied with harmony search (HS) and tabu search (TS) methods using the design algorithms developed for them in Hasançebi et al. (2009). When executed over the same number of function evaluations, a solution of 269,055.45 lb (122,043.55 kg) was achieved with HS method, whereas TS has resulted in a final design weight of 236,586.49 lb (107,315.63 kg), which is very close to that of iSA. These two designs are also reported in Table 3.

In Fig. 5, the variation of feasible best design obtained so far during the search is plotted against the number of function evaluations for the three variants of SA algorithm. In addition, the variation of average acceptance probability parameter in these runs is displayed in Fig. 6. As discussed in Section 4, the average acceptance probability at a cooling cycle is obtained by averaging the acceptance probabilities of all candidates subjected to Metropolis test at that cooling cycle. It is clear from these two figures that average acceptance probability in sSA has not been reduced to a level required for effective exploitative search. The fact that a high percentage of poor candidates are still accepted towards the end of the process has prevented the algorithm from convergence to favourable design regions. As a result, a randomized search was carried out mostly by allowing transitions in wide design regions. A refinement in the operation of Boltzmann parameter with transformed $\Delta\phi_{tra}$ values in pSA has recovered the situation in some measure. A better convergence characteristic was exhibited

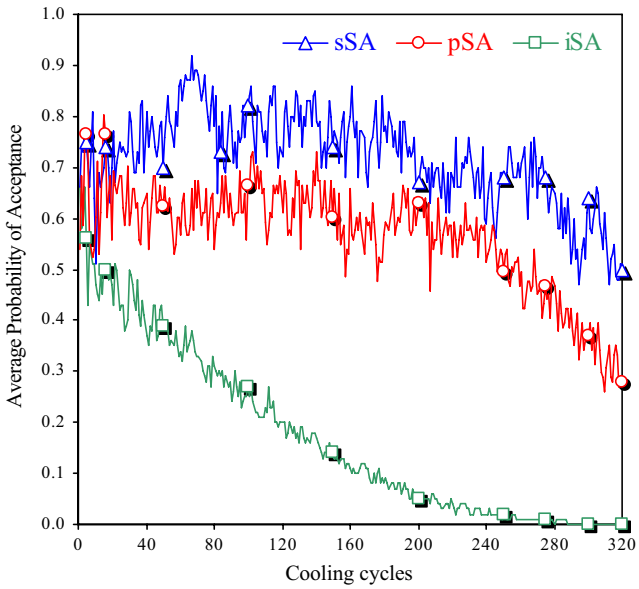

Fig. 6 The variation of average acceptance probability parameter in sSA, pSA and iSA algorithms for 304-member braced planar steel frame

by the algorithm under the effect of slightly aggravated transitions to non-improving regions, yet its performance was still far from being satisfactory. Besides the refinement of Boltzmann parameter, the use of correction factor ψ in iSA enforced the algorithm to keep track of the idealized (theoretical) acceptance probability curve as observed in Fig. 6. As a consequence of this, a rapid and reliable convergence of the algorithm was achieved towards the optimum.

5.2 Example 2: 132-member unbraced space steel structure

The second example shown in Fig. 7 is a three dimensional unbraced (swaying) steel frame consisting of 70 joints and 132 members that are grouped into 30 independent size variables (Fig. 7b) to satisfy practical fabrication requirements. The columns are selected from the complete W-shape profile list consisting of 297 ready sections, whereas a discrete set of 171 economical sections selected from W-shape profile list based on area and inertia properties is used to size beam members. Both gravity and lateral loads are considered in designing the frame. Gravity loads are calculated the using the same design considerations as in the previous example, yielding uniformly distributed loads on the outer and inner beams of the roof and floors given in Table 4. As for lateral forces, earthquake loads (E) are considered. These loads are computed as to equivalent lateral force procedure outlined in ASCE 7-05 (2005), resulting in the values given in Table 4 that are applied at the center of gravity of each story as joint loads. Gravity (G) and earthquake (E) loads are combined under two loading conditions for the frame: (a) 1.0G + 1.0E (in x-direction), and (b) 1.0G + 1.0E (in y-direction). The combined stress, stability and geometric constraints are imposed as explained in Section 2. The joint displacements in x and y direction are restricted to 1.53 in (3.59 cm) which is obtained as height of frame/400. Furthermore, story drift constraints are applied to each storey of the frame which is equal to height of each story/400.

Again the three variants of SA algorithm are tested to minimize the frame weight. Each algorithm is run a certain number of times independently, and only the best performances are considered. For sSS and pSA, the following control parameters are selected to sample approximately 50,000 designs during the search process: $P_s = 0.50$, $P_f = 10^{-7}$, $i_s = 1$, $i_f = 7$, $n_w = 10$, $N_c = 300$. The same values of parameter set are also used for iSA except that final acceptance probability is set to $P_f = 10^{-3}$. Once again the sSA algorithm exhibited a very poor performance, as anticipated. The lack of convergence characteristics has guided the casual search towards a final design weight of

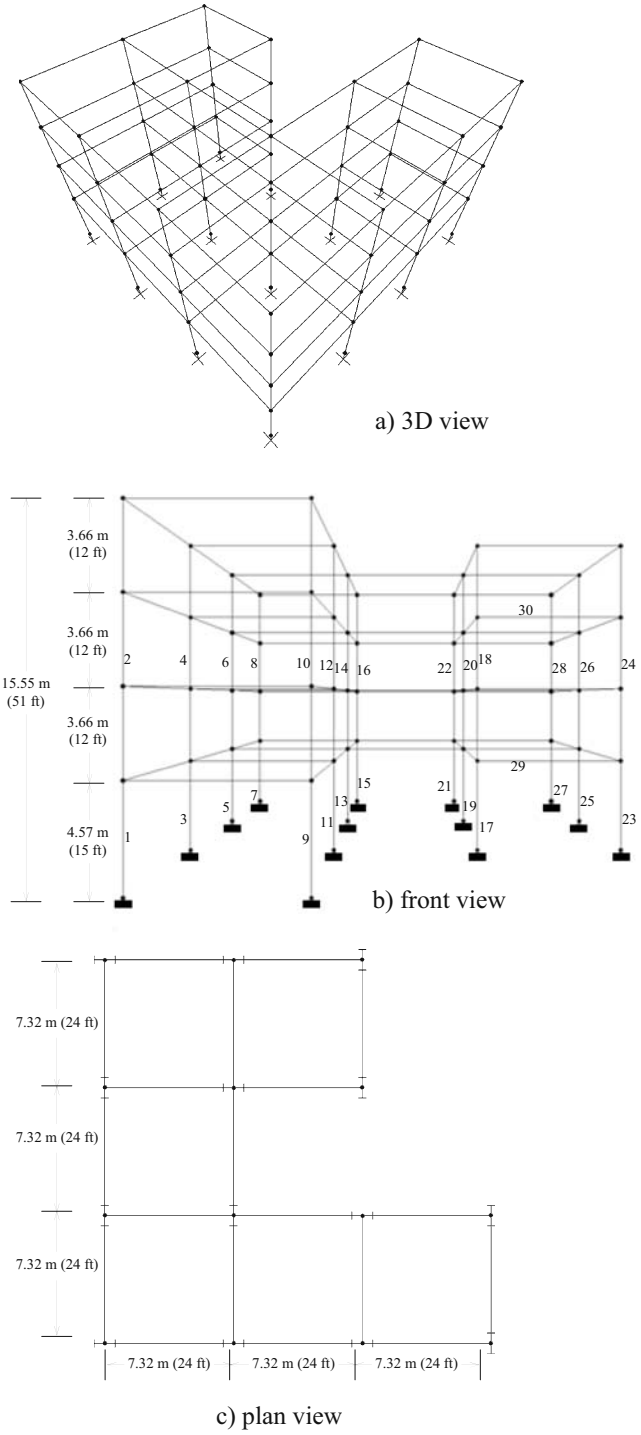

Fig. 7 132-member unbraced space steel frame **a** 3D view, **b** front view, **c** plan view

201,234.87 lb (91,280.14 kg) that is very far from the optimum. A certain improvement of this design was achieved with the proposed reformulation of Boltzmann parameter, such that pSA resulted in a final design of 148,590.60 lb

Table 4 The gravity and lateral loading on 132-member unbraced space steel frame

Beam type	Uniformly distributed load				Floor number	Earthquake design load	
	Outer span beams		Inner span beams				
	(lb/ft)	(kN/m)	(lb/ft)	(kN/m)		(kips)	(kN)
Gravity loads							
Roof beams (dead + snow loads)	1,011.74	14.77	1,193.84	17.42			
Floor beams (dead + live loads)	1,468.40	21.49	1,732.70	25.29			
Lateral loads							
					1	6.57	29.23
					2	12.43	55.28
					3	18.52	82.35
					4	24.76	110.15

Table 5 Final best designs of 132-member unbraced space steel frame obtained with iSA, TSO and HS methods

Size variables	iSA		TS		HS	
	Ready section	Area, $cm^2(in^2)$	Ready section	Area, $cm^2(in^2)$	Ready section	Area, $cm^2(in^2)$
1	W8X35	66.45(10.3)	W8X31	58.9 (9.13)	W14X53	100.65 (15.6)
2	W18X86	163.23 (25.3)	W12X65	123.33 (19.1)	W12X120	227.74 (35.3)
3	W12X79	149.68 (23.2)	W27X129	243.87 (37.8)	W30X48	280.65 (43.5)
4	W18X65	123.26 (19.1)	W8X58	110.32 (17.1)	W16X77	145.81 (22.6)
5	W12X65	123.26 (19.1)	W12X79	149.68 (23.2)	W18X119	226.45 (35.1)
6	W27X161	305.81 (47.4)	W12X106	201.29 (31.2)	W24X104	197.42 (30.6)
7	W24X117	221.94 (34.4)	W18X97	183.87 (28.5)	W30X148	280.65 (43.5)
8	W10X54	101.94 (15.8)	W8X58	110.32 (17.1)	W10X68	129.03 (20.0)
9	W18X86	163.23 (25.3)	W12X72	136.13 (21.1)	W18X158	298.71 (46.3)
10	W12X96	181.94 (28.2)	W14X90	170.97 (26.5)	W12X120	227.74 (35.3)
11	W10X60	113.55 (17.6)	W36X135	256.13 (39.7)	W36X150	285.16 (44.2)
12	W10X49	92.90 (14.4)	W10X49	92.90 (14.4)	W16X67	127.10 (19.7)
13	W12X87	165.16 (25.6)	W12X96	181.93 (28.2)	W10X112	212.26 (32.9)
14	W12X50	94.84 (14.7)	W10X49	92.90 (14.4)	W24X117	221.94 (34.4)
15	W24X55	104.52 (16.2)	W24X55	104.52 (16.2)	W18X40	76.13 (11.8)
16	W24X55	104.52 (16.2)	W10X33	62.65 (9.71)	W14X61	115.48 (17.9)
17	W12X58	109.68 (17.0)	W18X76	143.87 (22.3)	W12X65	123.23 (19.1)
18	W12X67	127.1 (19.7)	W21X83	156.77 (24.3)	W18X119	226.45 (35.1)
19	W12X40	76.13 (11.8)	W8X40	75.48 (11.7)	W14X82	155.48 (24.1)
20	W10X49	92.90 (14.4)	W14X61	115.48 (17.9)	W18X86	163.23 (25.3)
21	W12X72	136.13 (21.1)	W18X76	143.87 (22.3)	W14X90	170.97 (26.5)
22	W12X79	149.68 (23.2)	W12X72	136.13 (21.1)	W18X97	183.87 (28.5)
23	W8X48	90.97 (14.1)	W12X40	76.13 (11.8)	W21X73	138.71 (21.5)
24	W24X68	129.68 (20.1)	W24X76	144.52 (22.4)	W12X87	165.16 (25.6)
25	W14X61	115.48 (17.9)	W10X77	145.80 (22.6)	W18X71	134.19 (20.8)
26	W21X50	94.84 (14.7)	W16X50	94.84 (14.7)	W27X102	193.55 (30.0)
27	W8X40	75.48 (11.7)	W10X49	92.90 (14.4)	W8X48	90.97 (14.1)
28	W8X67	127.10 (19.7)	W14X61	115.48 (17.9)	W24X117	221.94(34.4)
29	W10X39	74.19 (11.5)	W18X97	183.87 (28.5)	W18X97	183.87 (28.5)
30	W21X44	83.87 (13.0)	W16X45	85.81 (13.3)	W16X40	76.13 (11.8)
Weight	138,874.67 lb	(62,993.55 kg)	142,710.96 lb	(64,733.69 kg)	143,135.29 lb	(64,926.17 kg)

(67,400.70 kg). The optimum design of the frame tabulated in Table 5 was attained with iSA again, and weighs 138,874.67 lb (62,993.55 kg) only. The attempts to optimize the frame with HS and TS methods over the same number of function evaluations yielded the slightly higher final design weights of 143,135.29 lb (64,926.17 kg) and 142,710.96 lb (64,733.69 kg), respectively, which are also tabulated in Table 4 for comparison purposes.

Figure 8 displays the variation of feasible best design in the best runs of the three variants of SA algorithm, whereas the variation of average acceptance probabilities in these runs is plotted in Fig. 9. Again an improvement in convergence characteristics of the algorithm by means of the proposed strategies can easily be observed from these two figures. It is noted that the effect of refinement of Boltzmann parameter is more pronounced for this example than the previous one. This argument can be verified by the observation that the degree of reformation of average acceptance probability parameter with pSA in Fig. 9 is remarkably higher than its corresponding curve in Fig. 6. This is also clear from the fact that although the final design weight reached with pSA in the first example is still very far from the optimum, it is somewhat higher than the optimum in the second example. The 3D geometry of the frame in the second example increases the problem complexity, plus especially geometric constraints become much more effective for this example. It follows that a vast number of extremely poor designs are generated during the course of the search process, and thereby the influence of refinement of Boltzmann parameter is better emphasized in the second example.

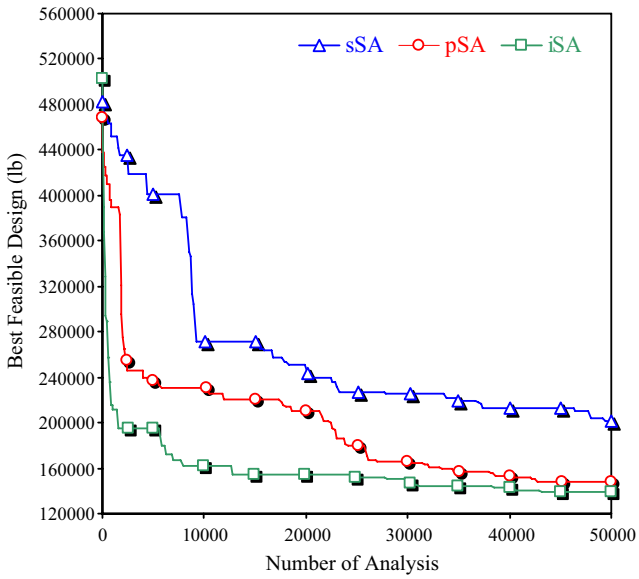

Fig. 8 The variation of feasible best design in sSA, pSA and iSA algorithms for 132-member unbraced space steel frame example

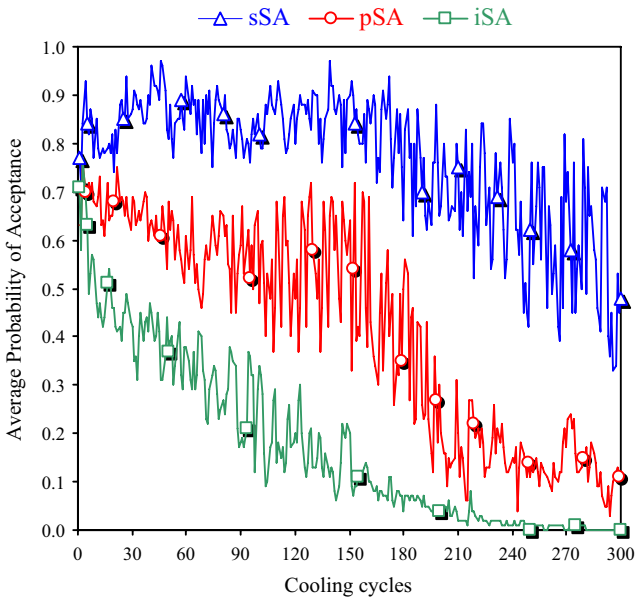

Fig. 9 The variation of average acceptance probability parameter in sSA, pSA and iSA algorithms for 132-member unbraced space steel frame example

6 Conclusions

This study is concentrated on enhancing performance of SA algorithm in real-size structural optimization applications with practical design considerations. It is emphasized and clearly demonstrated through the Figs. 2, 6 and 9 that when optimum design of such systems is required, the standard SA algorithm gets incongruous with theoretical consideration and faces serious convergence problems. Hence, a reformulation of the technique has been conducted by two generic parameters to eliminate the observed drawbacks of the standard algorithm. A correction term ψ is first defined in (20)–(21) to modify acceptance probability of a non-improving candidate based on observed value of average acceptance probability in theory and in practice. Secondly, a sigmoid function based transformation of $\Delta\phi$ values is proposed (21) for the update of Boltzmann parameter (22) to avoid the degeneration of the search process by extremely poor candidates. The resulting algorithm (iSA) has been tested and compared with the standard one (sSA) on two numerical examples (Figs. 4 and 7) chosen from size optimum design of large scale steel frameworks. The final designs obtained with iSA are lower than those of sSA as much as 35% in the first example and 31% in the second example. A comparison of optimum designs in Tables 3 and 5 appraises and evinces optimality of the solutions attained with iSA. The variations of average acceptance probability parameter in these examples are also plotted in Figs. 5 and 8 to rationalize enhancement in convergence

characteristics of the algorithm. It has been found that the correction term ψ is mainly responsible for the improvement achieved in the first example, whereas refinement of Boltzmann parameter seems to be more effective in the second one.

Acknowledgements This paper is partially based on research supported by the Scientific Research Council of Turkey (TUBITAK Research Grant No: 108M070) and the Middle East Technical University Research Funding (BAP-2008-03-03-02), which are gratefully acknowledged.

Appendix

Notation List:

A_i	area of the steel section adopted for member group i
b_{fb}	flange width of a beam
b_{fc}	flange width of a column
C_{mx}	a reduction factor to counterbalance overestimation of the effect of secondary moments
C_{my}	a reduction factor to counterbalance overestimation of the effect of secondary moments
C_v	web shear coefficient
d_c	depth of a column
E	elasticity modulus
f_a	computed axial stress
f_{bx}	computed flexural stress due to bending of the member about its major (x) axis
f_{by}	computed flexural stress due to bending of the member about its minor (y) axis
f_v	computed shear stress
F_a	allowable axial stress under axial compression force alone
F_{bx}	allowable bending compressive stress about major (x) axis
F_{by}	allowable bending compressive stress about minor (y) axis
F'_{ex}	Euler stress about principal x-axis of a member
F'_{ey}	Euler stress about principal y-axis of a member
F_v	allowable shear stress
F_y	material yield stress
g_i	i-thproblem constraint
G_A	stiffness ratio or relative stiffness of a column at one end
G_B	stiffness ratio or relative stiffness of a column at the other end
h	clear distance between flanges
h	height of a story
H	total height of the frame building
i_c	iteration of a cooling cycle
i_f	iteration of final cooling cycle
i_s	iteration of starting cooling cycle
I_i	current value of i-th design variable
I'_i	perturbed value of i-th design variable
$\mathbf{I}$	a design vector of integer values representing the sequence numbers of steel sections assigned to member groups
K	effective length factor
K	Boltzmann parameter
$K^{(p)}$	Boltzmann parameter value before update
$K^{(u)}$	updated value of Boltzmann parameter
L_j	length of the member j which belongs to group i
n_w	width of the neighborhood
N_a	number of previous poor candidates
N_c	number of cooling cycles
N_d	number of design groups (variables)
N_m	number of members in a structural system
N_t	total number of members in group i
P	acceptance probability of a poor candidate
P_s	starting acceptance probability
P_f	final acceptance probability
$\left(\overline{P}_t\right)^{(k-1)}$	theoretical average acceptance probability at the $(k-1)$-th cooling cycle
$\left(\overline{P}_p\right)^{(k-1)}$	practical (operational) average acceptance probability at the $(k-1)$-th cooling cycle
r	radii of gyration of a member
t_f	flange thickness of a column
t_w	thickness of web
T_f	final temperature
T_s	starting temperature
T^k	temperature at k-th cooling cycle
W	weight of the frame
z_i	amount of perturbation applied to the i-th design variable
ρ_i	unit weight of the steel section adopted for member group i secondary moments
λ	slenderness ratio
η	cooling factor
ϕ	constrained objective function value
ϕ_c	constrained objective function value of current design
ϕ_a	constrained objective function value of candidate (alternative) design
α	penalty coefficient
$\Delta\phi$	difference between the objective function values of current and candidate designs
ψ	correction factor in acceptance probability
$\Delta\phi_{tra}$	transformed value of $\Delta\phi$

References

AISC-ASD (1989) Manual of steel construction—allowable stress design, 9th edn. Chicago, Illinois, USA

AISC-LRFD (1986) Manual of steel construction—load and resistance factor design SA

ANSI/AISC 360-05 (2005) Specification for structural steel buildings. Chicago, Illinois, USA

ASCE 7-05 (2005) Minimum design loads for building and other structures

Balling RJ (1991) Optimal steel frame design by simulated annealing. J Struct Eng 117(6):1780–1795

Bennage WA, Dhingra AK (1995) Single and multiobjective structural optimization in discrete-continuous variables using simulated annealing. Int J Numer Methods Eng 38:2573–2773

Ceramic B, Fryer C, Baires RW (2001) An application of simulated annealing to the optimum design of reinforced concrete retaining structures. Comput Struct 79:1569–1581

Chen T-Y, Su J-J (2002) Efficiency improvement of simulated annealing in optimal structural designs. Adv Eng Softw 33:675–680

Chen G.-S, Bruno RJ, Salama M (1991) Optimal placement of active/passive members in truss structures using simulated annealing. AIAA J 29(8):815–827

Değertekin SÖ (2007) A comparison of simulated annealing and genetic algorithm for optimum design of nonlinear steel space frames. Struct Multidiscipl Optim 34:347–359

Dumonteil P (1992) Simple equations for effective length factors. Eng J AISC 29(3):111–115

Erdal O, Sönmez FO (2005) Optimum design of composite laminates for maximum buckling load capacity using simulated annealing. Compos Struct 71:45–52

Glover F (1989) Tabu search-part I. ORSA J Comput 1(3): 190–206

Hasançebi O, Erbatur F (2001) On efficient use of simulated annealing in complex structural optimization problems. Acta Mech 157: 27–50

Hasançebi O, Erbatur F (2002) Layout optimisation of trusses using simulated annealing. Adv Eng Softw 33:681–696

Hasançebi O, Çarbaş S, Doğan E, Erdal F, Saka MP (2009) Performance evaluation of metaheuristic search techniques in the optimum design of real size pin jointed structures. Comput Struct 87(5–6):284–302

Hellesland J (1994) Review and evaluation of effective length formulas. Research Report, ISBN 82-553-0930-6, No. 94-2, University of Oslo

Kirkpatrick S, Gelatt CD, Vecchi MP (1983) Optimization by simulated annealing. Science 220:671–680

Lamberti L (2008) An efficient simulated annealing algorithm for design optimization of truss structures. Comput Struct 86:1936–1953

Lee KS, Geem ZW (2004) A new structural optimization method based on the harmony search algorithm. Comput Struct 82:781–798

Moh J-S, Chiang D-Y (2000) Improved simulated annealing search for structural optimization. AIAA J 38(10):1965–1973

Shim PY, Manoochehri S (1997) Generating optimal configurations in structural design using simulated annealing. Int J Numer Methods Eng 40:1053–1069

Sönmez FO (2007) Shape optimization of 2D structures using simulated annealing. Comput Methods Appl Mech Eng 196:3279–3299

Tzan S-R, Pantelides CP (1996) Annealing strategy for optimal structural design. J Struct Eng 122(7):815–827